Reaction Chemistry & Engineering

ROYAL SOCIETY OF CHEMISTRY

PAPER

View Article Online
View Journal | View Issue

Cite this: *React. Chem. Eng.*, 2024, **9**, 439

Tracking sodium cobaltate formation pathways and its CO_2 capture dynamics in real time with synchrotron X-ray diffraction†

Federico Hector Cova *[a] and Maria Valeria Blanco *[b]

Received 30th August 2023,
Accepted 30th October 2023

DOI: 10.1039/d3re00459g

rsc.li/reaction-engineering

Na-based high temperature CO_2 solid sorbents hold great potential for capturing the CO_2 emitted by large stationary sources. However, to benefit from these materials in schemes of CO_2 capture, simple synthesis procedures together with a comprehensive understanding of their behaviour under operative conditions is essential. In this work, we use time-resolved *in situ* synchrotron X-ray diffraction coupled with Rietveld analysis to investigate the synthesis and high temperature CO_2 capture dynamics of $NaCoO_2$ solid sorbent. $NaCoO_2$ was synthesized *via* two different routes, from $CaCO_3{\cdot}H_2O$ and Na_2CO_3 and from Co_3O_4 and Na_2CO_3 reactants, and a comparative analysis of the temperature-dependent phase transformations occurring during each synthesis reaction and their effect on the final product allowed to identify the most efficient synthesis route. The reaction mechanism between $NaCoO_2$ and CO_2 in the temperature range between 50 °C and 750 °C at 1 bar of CO_2 is also provided. The results on the fundamental aspects underpinning $NaCoO_2$ synthesis and its CO_2 capture dynamics under realistic operative conditions are key for the design and development of affordable CO_2 solid sorbents.

Greenhouse gas emissions are pinpointed as the key driver of global warming and therefore responsible for the changes observed in the climate, which are unprecedented in thousands of years and which have set in motion far-reaching massive effects on ecosystems, bringing immeasurable ecological, economical and social negative impacts.[1–5] Among greenhouse gases of varying lifetimes contributing to climate change, the great persistence displayed by CO_2 renders its warming practically irreversible for more than 1000 years.[6] Because of this, strong and sustained reductions in emissions of CO_2 are an imperious need.

Society is confronted with the important objective of achieving carbon neutrality on a global scale. While there is widespread agreement that electromobility is leading the charge in decarbonizing transportation, finding viable solutions for other industrial sectors proves to be a significant challenge. In cases where electrification is not feasible, it becomes essential to explore technological advancements that can effectively prevent CO_2 emissions from being released into the atmosphere. Considering that power plants contribute to 40% of human-caused CO_2 emissions,[7] the development and implementation of engineering solutions capable of capturing CO_2 from high-temperature flue gases in large stationary sources, such as power stations and industrial plants, emerge as a promising avenue for mitigating CO_2 gas emissions.

Many ceramic compounds are able to react with CO_2 at high temperatures, and this occurs *via* a two-step temperature dependent gas–solid reaction. At low temperatures, CO_2 reacts at the surface of the material producing a carbonated shell, and at high temperatures the reaction proceeds through the bulk of the particles. The captured carbon can be later utilized as a valuable feedstock for industrial chemical production. Within ceramic compounds, Lithium containing materials have shown high CO_2 sorption capacity, together with good reversibility over a wide temperature operation range.[5]

Li_4SiO_4 is one of the most studied systems for high temperature CO_2 capture applications,[8–10] exhibiting a high CO_2 sorption capacity of 0.367 g_{CO_2} $g_{sorbent}^{-1}$, low regeneration temperatures (<750 °C), and remarkable sorption/desorption cycling stability, which ensures a long operational lifetime under realistic conditions.[11] However, despite Li_4SiO_4 excellent CO_2 capture properties, the growing demand of Li to fulfil the needs of other technological applications, such as Lithium-ion batteries, along with the fact that it is not highly abundant has given rise to a serious concern about Li long-term availability[12] and creates the need to explore more accessible, cheap and sustainable materials for CO_2 sorbents.

[a] *ALBA CELLS, Carrer de la Llum 2-26, Barcelona, 08290 Cerdanyola del Vallés, Spain. E-mail: fcova@cells.es*
[b] *Aragon Institute of Nanosciences and Materials, University of Zaragoza, C/ Pedro Cerbuna, 12 50009, Zaragoza, Spain. E-mail: mariavaleria.blanco@unizar.es*
† Electronic supplementary information (ESI) available. See DOI: https://doi.org/10.1039/d3re00459g

Partial replacements of lithium by sodium in Li_4SiO_4 ceramic in the form of solid solutions of $Li_{4-x}Na_xSiO_4$ have shown an enhancement of CO_2 absorption kinetics compared to pure Li_4SiO_4, together with increased CO_2 absorption.[13] This indicates that Na atoms act as active sites for CO_2 capture reactions. Furthermore, complete replacements of Li by Na, leading to the Na_4SiO_4 structure, have shown improved CO_2 capture performance in terms of high temperature sorption and desorption compared with Li_4SiO_4.[14]

Na_2CO_3, Na_2ZrO_3 and $NaCoO_2$ are promising options for obtaining lithium-free CO_2 solid sorbents.[15–19] A recent study showed the great ability of $NaCoO_2$ to catalyze the conversion of CO to CO_2 and to subsequently chemisorb the latter.[20] $NaCoO_2$ compounds are comprised of hexagonal CoO_2 blocks and a Na layer, forming a layered oxide material. Notably, the Na layer exhibits a high degree of vacancy, leading to variations in the crystal structure depending on the Na content. Such unique structure consisting of layered hexagonal blocks with alkaline elements is expected to allow for easy diffusion and improved chemisorption of CO_2, and the introduction of structural defects can be used as an strategy to modify the diffusion processes. Therefore, the crystalline structure of the material plays a crucial role in enhancing the diffusion of sodium during the CO_2 chemisorption process. Furthermore, the presence of cobalt in this ceramic may induce catalytic activity in the CO oxidation reaction. Based on these findings, efforts have been dedicated to understand the chemical reactions that this material undergo at high temperatures.[18–20]

Results from *ex situ* X-ray diffraction studies suggest that upon carbonation $NaCoO_2$ would transform to Na_2CO_3 and cobalt oxides, Co_3O_4 and CoO. While these findings provide support for the reactivity of $NaCoO_2$ towards CO_2, the presence of such cobalt oxides suggests a change of cobalt valence, indicating a complex CO_2 capture process involving not only surface and diffusion reactions but also electronic exchanges. This *ex situ* evidence provokes the need of a comprehensive understanding on how $NaCoO_2$ behaves in the presence of CO_2 in the temperature range that is of interest for CO_2 capture applications, which is critical to evaluate its performance under real working conditions and to determine its regeneration potential. This requires the use of *in situ* advanced characterization techniques.

X-ray diffraction analysis (XRD) has been widely used for identifying crystallographic phases after high-temperature CO_2 experiments, and *in situ* XRD experiments have proven to be particularly beneficial for monitoring the chemical reactions and morphological changes that sorbents undergo upon carbonation.[21–25] Moreover, the advanced capabilities of synchrotron facilities, including their high brilliance and detection capabilities, have enabled the performance of time-resolved synchrotron XRD studies. This cutting-edge approach allows for the dynamic behavior of materials at elevated temperatures to be tracked with a resolution of seconds, allowing to reveal the appearance of intermediate phases and the occurrence of re-conversion processes which would not be possible to detect using standard laboratory sources.[26–29] Hence, time-resolved high temperature synchrotron analysis on the carbonation reactions of $NaCoO_2$ sorbent would bring unique insights on its reaction mechanism with CO_2 under operative conditions and would provide solid grounds to analyze its potential use as CO_2 solid sorbent for real applications.

Owing to its promising properties as a CO_2 sorbent and its excellent performance as cathode for rechargeable sodium batteries,[30–32] there is also a general interest in improving $NaCoO_2$ synthesis conditions. Among the many reported synthesis methods, the solid-state route is a well-established and simple procedure to synthesize $NaCoO_2$ structures. Reddy and co-workers have shown to obtain hexagonal P2-$NaCoO_2$ through the calcination of mixed stoichiometric amounts of CH_3COONa, $Co(CH_3COO)_2{\cdot}4H_2O$ and glycine at 800 °C. Also, in a recent work,[33] P2-$NaCoO_2$ was synthesized by solid state reaction from Na_2CO_3 and Co_3O_4 heat treated at 850 °C for 24 h under air flow. Other works used reactive Na_2O_2 and Co_3O_4 as starting reactants and performed different heat treatments at temperatures ranging from 450 °C to 750 °C.[34] Hence, due to the multiple methods that have been reported for the synthesis of $NaCoO_2$ and the need to use cheap and benign precursors, more thorough investigations are required.

To provide a comprehensive assessment of the potential use of $NaCoO_2$ as CO_2 sorbent material, this study focuses on two main aspects. Firstly, we perform a comparative investigation of two thermally driven synthesis routes for obtaining this material at the lower possible temperature from simple reactants using time-resolved synchrotron powder X-ray diffraction coupled with Rietveld analysis. Later, we analyze in real time the structural changes of $NaCoO_2$ under CO_2 flow in the temperature range from 30 °C to 750 °C. *In situ* X-ray diffraction coupled with Rietveld analysis allowed to identify reaction products and to propose a simple reaction mechanism, which is different from the one proposed on the basis of previous *ex situ* XRD results. The results from this work are crucial for the efficient synthesis of $NaCoO_2$ and provide solid grounds of its reaction mechanism as CO_2 sorbent and its regeneration capability.

1. Experimental

1.1. *In situ* synthesis of $NaCoO_2$

$NaCoO_2$ was synthesized *via* two solid-state routes. In the first synthesis route, powders of Na_2CO_3 (99.5%, Sigma Aldrich) and $CoCO_3{\cdot}xH_2O$ (99.9%, Sigma Aldrich) were used as reactants, whereas in the second synthesis $NaCoO_2$ was produced from Na_2CO_3 and Co_3O_4 (99.9%, Sigma Aldrich). Based on preliminary results, 20 wt% excess of the sodium source was added to the mixture to compensate Na losses due to sublimation, which is in line with previous publications.[20] Reactant powders were mechanically mixed in a Retsch shaker for 5 minutes, then loaded into a 1 mm

quartz capillaries and heated up under synthetic air flow from room temperature to 800 °C at a ramp rate of 5 °C min^{-1}. Temperature inside the capillary was measured constantly during the experiment using a thermocouple in direct contact with the sample. Another thermocouple was located on the outside of the capillary of control the temperature of the hot nitrogen stream provided by the gas blower to heat the system. In the first synthesis 30 min isothermal conditions were kept after each 50 °C increment, whereas in the second synthesis the temperature was constantly increased without any isothermal step.

Time-resolved *in situ* synchrotron X-ray powder diffraction measurements were performed during both synthesis reactions. A sketch of the experimental setup can be found elsewhere.[27] Experiments were performed at the High-energy X-ray Diffraction Beamline ID31 of the European Synchrotron Radiation Facility (ESRF). Data collection time was 2 seconds, and the time resolution was of 30 seconds. Data was acquired using a Pilatus Dectris 2 M CdTe detector, at a wavelength was of 0.1771 Å and 0.1589 Å, and with a beamsize of 0.6 mm × 0.6 mm ($V \times H$). Data was processed using pyFAI package[35] and Rietveld analysis was performed using Fullprof suite software.[36]

1.2. *In situ* $NaCoO_2$ CO_2 capture

$NaCoO_2$ powder was loaded into a 1 mm quartz capillary. The inlet of the capillary was connected to a gas rig system that allowed the feed of a 10 mL min^{-1} flow of $CO_2:N_2$ (50 : 50) gas mixture to the sample and a continuous monitoring of the gas pressure. The capillary was horizontally placed on top of a gas blower that enabled the controlled heating and cooling of the sample in the temperature range from 30 °C to 750 °C at a ramp rate of 5 °C min^{-1}.

2. Results

2.1. $NaCoO_2$ from Na_2CO_3 and $CoCO_3{\cdot}xH_2O$

In Fig. 1a is displayed a contour plot with the X-ray diffraction patterns collected during the high-temperature synthesis reaction of $NaCoO_2$ from monoclinic Na_2CO_3 (m-Na_2CO_3) and $CoCO_3{\cdot}xH_2O$. The miller indices of the main phases present at different stages of the synthesis process are indicated within the graph. The evolution of temperature during the synthesis is depicted in Fig. 1b. The vertical axis of Fig. 1b is scaled in order to match the evolution of the diffractograms presented in Fig. 1a.

As temperature increases during the initial heating process, the reflections associated with the starting phases undergo a noticeable shift towards lower angles. This shift is a result of the thermal expansion of the respective lattices due to the temperature rise.

A first phase transition is observed at 240 °C. At this temperature, $CoCO_3$ decomposes into Co_3O_4 and CoO. This reaction must be accompanied by a release of CO_2. Interestingly, CoO rapidly reacts with oxygen coming from the synthetic air stream and is converted to Co_3O_4. According to previous reports,[37] at 240 °C this intermediate reaction that results in the formation of CoO is not thermodynamically favoured against the one that results on its complete transformation into Co_3O_4. However, the presence of CoO is clear in the diffraction patterns. This is an indication that the conversion is being affected by kinetic and/or diffusion limitations, which introduce this intermediate reaction. In this regard, it is worth noting that previous thermogravimetric analysis conducted on the heating of $CoCO_3$ (ref. 38) in air atmosphere based on the assumption of the chemical reaction $6CoCO_3 + O_2 \rightarrow 2Co_3O_4 + 6CO_2$ showed weight losses higher than the theoretical

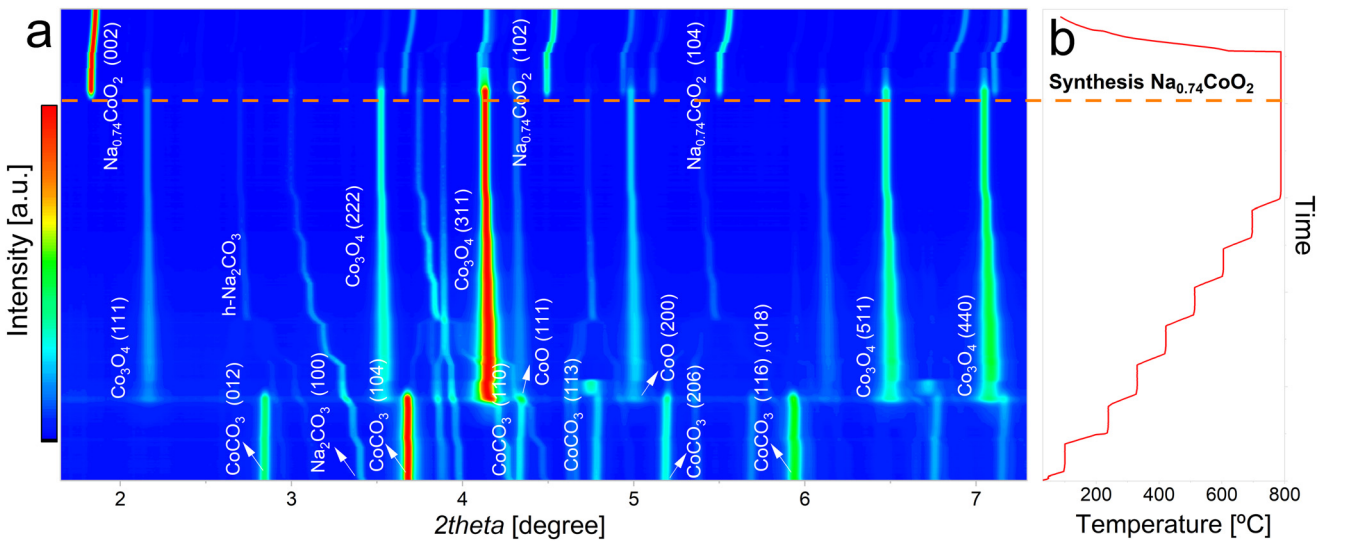

Fig. 1 a) Contour plot of the XRD patterns collected during the synthesis of $NaCoO_2$ from $CoCO_3$ and m-Na_2CO_3 precursors, b) evolution of the temperature and time during the synthesis process.

ones. These results could be explained considering the intermediate transition of $CoCO_3$ to Co_3O_4 + CoO + CO_2.

At 240 °C a coexistence of four phases, *m*-Na_2CO_3, $CoCO_3{\cdot}xH_2O$, $CoCO_3$ and CoO, is evidenced. At slightly higher temperatures, the reflections belonging to the $CoCO_3$ phase completely vanish. Further heating until 480 °C provokes a phase transition of Na_2CO_3 from monoclinic to an hexagonal crystal structure (*h*-Na_2CO_3). This high temperature phase transition was previously reported to occur above 400 °C (ref. 39) and has shown reversibility upon cooling.[40] At temperatures above 480 °C, the only phases present are *h*-Na_2CO_3 and Co_3O_4.

At 770 °C, both phases are expected to react to form $NaCoO_2$ through the following reaction:

$$2Na_2CO_3 + 4CoCO_3 + O_2 \rightarrow 4NaCoO_2 + 6CO_2$$

However, the *in situ* XRD results showed that the phase $Na_{0.74}CoO_2$ is formed, as it can be observed both from the refined crystal structure (Fig. 2f) and from comparison with previous results,[41] indicating the following reaction:

$$0.74Na_2CO_3 + 2CoCO_3 + 0.63O_2 \rightarrow 2Na_{0.74}CoO_2 + 2.74CO_2$$

This synthesis occurs immediately, the formation of a phase with vacancies in the Na site has been widely reported in previous experiments.[20] At 800 °C no further phase transformations are observed, and no residues from *h*-Na_2CO_3 and Co_3O_4 are evidenced, meaning that the reaction is completed. Once the synthesis is completed, the sample was cooled down at a rate of 10 °C min^{-1}. The shifts to the right of the peaks corresponding to the $Na_{0.74}CoO_2$ phase are due to cooling down of the sample.

In Fig. 2 are shown selected XRD patterns corresponding to six different stages of the synthesis process, together with their respective Rietveld refinement fitting results. Starting Na_2CO_3 and $CoCO_3{\cdot}xH_2O$ exhibit a monoclinic *C*12/*m*1 (JCPDS 01-077-2082) and rhombohedral $R\bar{3}c$ (JCPDS 01-078-0209) structures, respectively. At 300 °C these two structures are still preserved, but the cobalt carbonate suffers a disproportion to cubic Co_3O_4 $Fd\bar{3}m$ (JCPDS 01-076-1802) and cubic CoO $Fm\bar{3}m$ (JCPDS 00-009-0402). At this stage the phase percentages obtained by Rietveld analysis yielded the following results: 28.8 wt% Na_2CO_3, 31.6 wt% $CoCO_3$, 16.9 wt% Co_3O_4 and 22.7 wt% CoO. Further heating leads to the complete transformation of cobalt-based phases to Co_3O_4, with a phase composition of 48.4 wt% Na_2CO_3 and 51.6 wt%

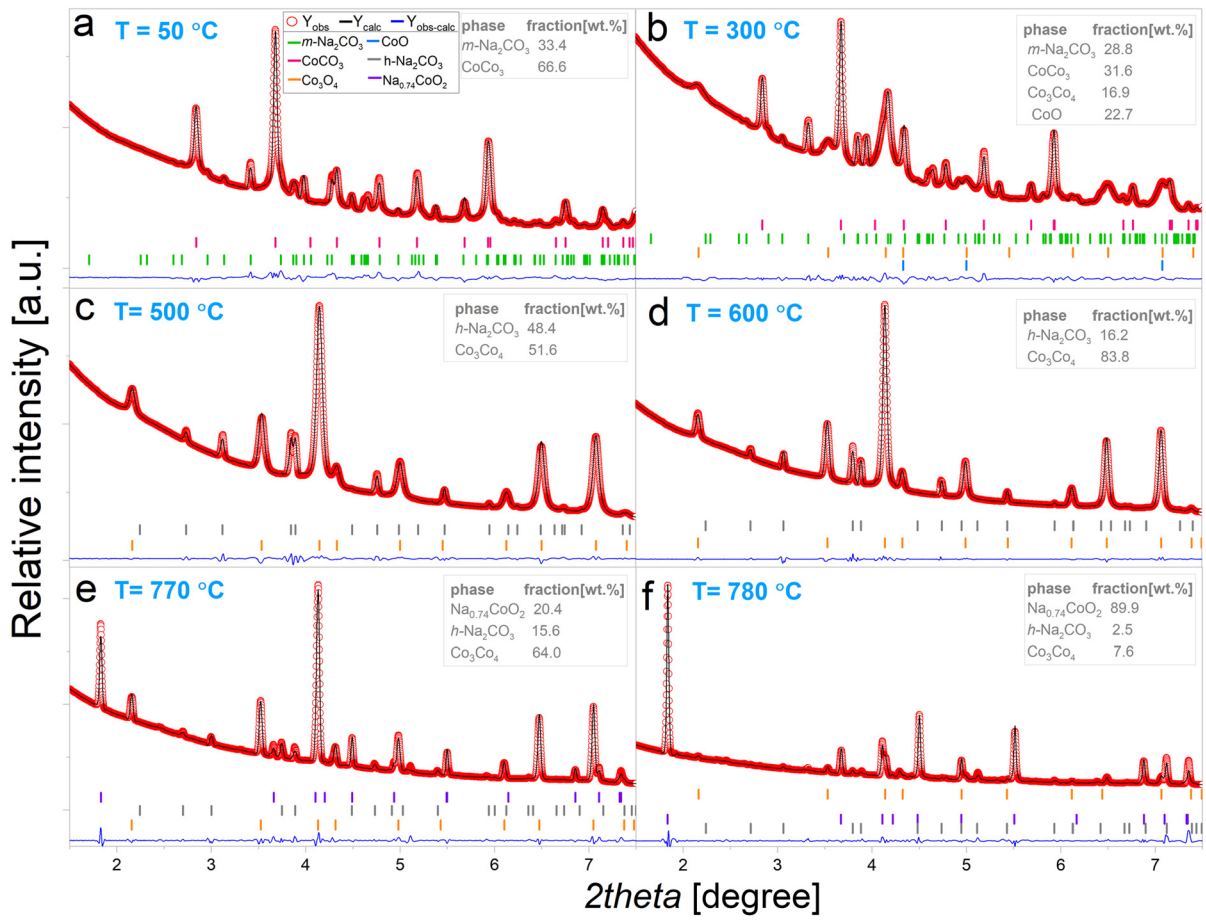

Fig. 2 Experimental X-ray diffraction patterns and results of the fittings performed using the Rietveld method for data collected at: a) 50 °C, b) 300 °C, c) 500 °C, d) 700 °C, e) 770 °C and f) 780 °C during $NaCoO_2$ synthesis process. Values of the refined parameters are presented at Tables S1A–F in ESI.†

Co_3O_4, and Na_2CO_3 transforms from monoclinic $C12/m1$ to hexagonal $P63/mmc$ structure (JCPDS 01-009-8623).

Further heating up to 600 °C results in a significant growth h-Na_2CO_3 grain domains, as it can be observed from the more defined and pronounced diffraction peaks of Fig. 2d. In Fig. 2e are depicted the XRD pattern corresponding to a phase coexistence between Co_3O_4, h-Na_2CO_3 and $NaCoO_2$, with a phase percentage of 64.0 wt%, 15.6 wt% and 20.4 wt%, respectively. Fig. 2f shows the state of the system at 780 °C, where the reaction is not fully completed but most of the system has transformed to $Na_{0.74}CoO_2$. The reported experimental results demonstrate that $NaCoO_2$ ($Na_{0.74}CoO_2$) can be synthesized at 780 °C, which is a temperature 70 °C lower than the reported in the literature using the same reactants.[20]

2.2. *In situ* $NaCoO_2$ synthesis from Na_2CO_3 and Co_3O_4

$NaCoO_2$ was also synthesized from Na_2CO_3 and Co_3O_4 powders. This synthesis route was previously used by Krasutskaya and co-workers.[42] In the proposed method, powder precursors were first mixed and grinded using an agate mortar and the resulting powder mixture was pressed at 40 MPa to produce pellets, which were then fired at 860 °C in air for 12 h. In their work, the authors used a Na : Co ratio of 1.2× : 1. This excess of Na_2CO_3 in the starting mixture compensates for the Na_2O loss during the high temperature heat treatment. In another work,[43] $NaCoO_2$ was synthesized from the same reactants, but using a procedure in which the powder mixture was grinded manually in an agate mortar for 2 h, then loaded into an alumina crucible and subsequently sintered three times at 860 °C in air. In such synthesis procedure, intermediate grinding was performed in a moisture-free atmosphere inside a glove box to obtain an homogeneous composition. Therefore, the total sintering time was of 36 h.

In this work, the synthesis was performed by heating the mixture of oxides with a ramp of 5 °C min^{-1} without any isothermal step. In Fig. 3 it can be observed that m-Na_2CO_3 and Co_3O_4 are the main phases present from room temperature until 200 °C, temperature at which Co_3O_4 evolves towards the formation of Co_2O_3. The initial composition is presented in Fig. 4a and the coexistence of the three mentioned phases is clearly observed in Fig. 4b. The presence of Co_2O_3 phase was not expected, since this phase is thermodynamically unstable, however, Fig. 4c indicates a significant amount of this phase at 450 °C. As can be seen from Fig. 3, the temperature range at which this particular phase exists is narrow, and Co_2O_3 swiftly reverts to Co_3O_4 upon further heating. At 550 °C, Fig. 4d this reversion is fully completed, leading to Co_3O_4 becoming the dominant phase in the system. From this temperature onwards, Na_2CO_3 and Co_3O_4 are the main components, although now m-Na_2CO_3 has transitioned to h-Na_2CO_3, as it was reported in the previous synthesis process. Finally, reflections corresponding to $Na_{0.74}CoO_2$ phase emerge at 690 °C as observed in Fig. 4e. At 700° only 12 wt% of $Na_{0.74}CoO_2$ is present on the sample, and after 20 min of isothermal conditions at this temperature, Fig. 4f, the synthesis reaction reaches completion. After 1 h of isothermal conditions the system remains stable, with 3.6 wt% of h-Na_2CO_3 detectable as impurity.

According to the results, $Na_{0.74}CoO_2$ is formed according to the following chemical reaction:

$$0.74Na_2CO_3 + 0.667Co_3O_4 + 0.297O_2 \rightarrow 2Na_{0.74}CoO_2 + 0.74CO_2$$

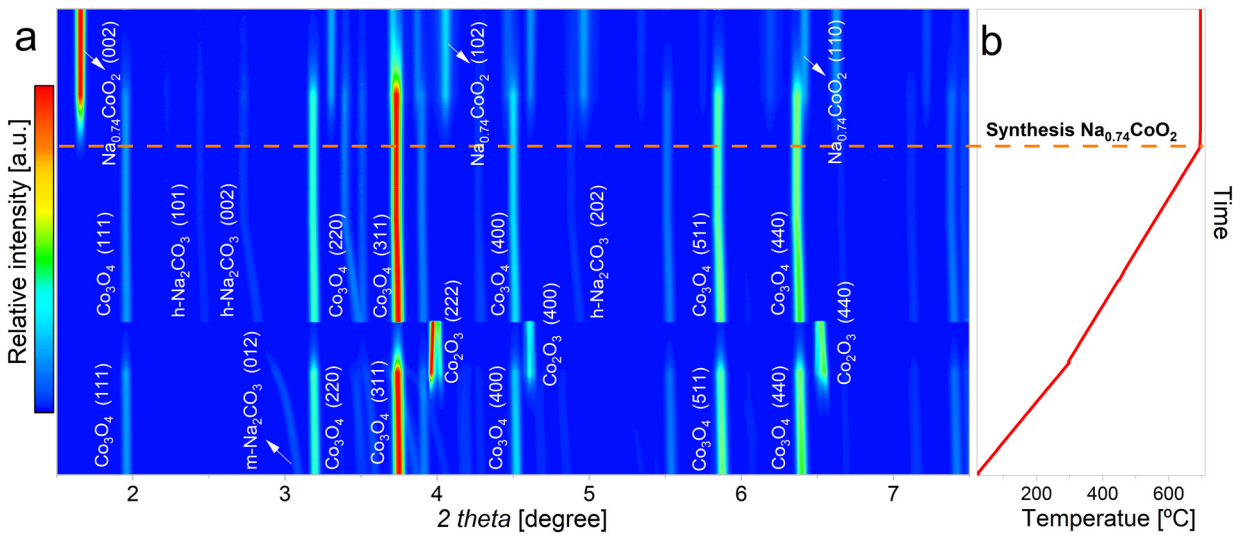

Fig. 3 a) Contour plot of the XRD patterns collected during the synthesis of $NaCoO_2$, starting from m-Na_2CO_3 and Co_3O_4 powders, b) temperature evolution during the solid-state synthesis of $NaCoO_2$.

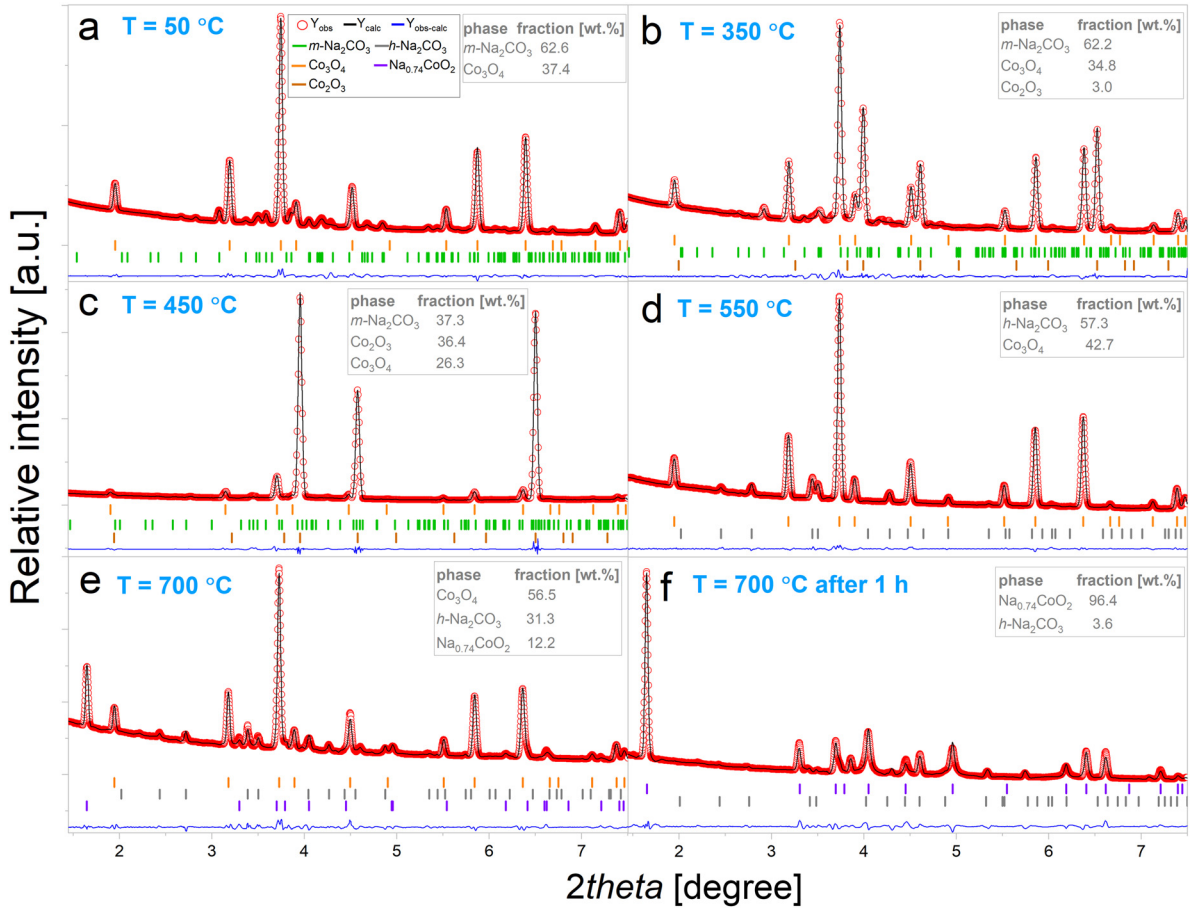

Fig. 4 Experimental X-ray diffraction patterns and results of the fittings performed using the Rietveld method for data collected at: a) 50 °C, b) 350 °C, c) 450 °C, d) 550 °C, e) 700 °C and f) 700 °C after 1 h of isothermal conditions during $NaCoO_2$ synthesis process. Values of the refined parameters are presented at Tables S2A–F in ESI.†

Which reveals again the presence of Na vacancies on the reaction product.

The synthesis of $Na_{0.74}CoO_2$ from *m*-Na_2CO_3 and Co_3O_4 reactants shows a $Na_{0.74}CoO_2$ formation temperature of about 100 °C lower compared with the solid state route involving the use of Na_2CO_3 and $CoCO_3{\cdot}H_2O$ precursors. Comparing the *in situ* XRD data of both synthesis processes, it becomes clear that the difference observed in the synthesis temperature of $Na_{0.74}CoO_2$ comes from the need of an intermediate stage in the first synthesis method, in which the $CoCO_3$ transitions towards Co_3O_4, a step that requires higher temperature and energy input.

Overall, the lower synthesis temperature observed in the reaction between Na_2CO_3 and Co_3O_4 suggests a more efficient and potentially cost-effective route for the production of sodium cobaltate compared to the solid-state method involving *m*-Na_2CO_3 and $CoCO_3{\cdot}H_2O$ as precursors. It must also be emphasized that the reported synthesis temperature for a sodium cobalate from *m*-Na_2CO_3 and Co_3O_4 is 150 °C lower than temperatures reported in the literature using the same reactants.

2.3. CO_2 capture

Previous research on sodium and lithium ceramics suggests that a reaction between $NaCoO_2$ and CO_2 would occur according to the following route:[19,20]

$$2NaCoO_2 + CO_2 \rightarrow Na_2CO_3 + Co_2O_3$$

However, Co_2O_3 reaction product is a highly unstable compound according to thermodynamics and has been rarely observed outside very particular conditions,[44,45] so its formation during the absorption process is highly unlikely, although it may be possible for it to appear as an intermediate product for shorts amounts of time before decomposing into O_2 and Co_3O_4.

In a study conducted by Vera *et al.*,[20] the dynamic thermogram of $NaCoO_2$ under CO_2 flow was measured and displayed a continuous weight gain between 150 °C and 740 °C. This weight gain was divided into two temperature ranges: (i) 180–415 °C, corresponding to the superficial CO_2 chemisorption process, and (ii) 415–740 °C, corresponding to the bulk CO_2 chemisorption process. The authors analyzed *ex situ* XRD samples of CO_2NaCoO_2 isothermal reaction

products and observed significant structural modifications of $NaCoO_2$ at 400 °C, which were attributed to partial sodium release and subsequent formation of Co_3O_4. As the temperature increased further, between 450 °C and 700 °C, reflections belonging to $NaCoO_2$ phase gradually disappeared, diffraction peaks corresponding to Na_2CO_3 phase emerged and reflections corresponding to Co_3O_4 phase became stronger. Interestingly, at temperatures exceeding 700 °C, the authors evidenced the presence of CoO phase. These findings contradicted previous literature proposing the presence of a different cobalt oxide, Co_2O_3, based on the assumption that cobalt retains its +3 valence state. Hence, Vera and coworkers claim that the valence of cobalt changes from +3 to +2, as indicated by the presence of Co_3O_4 and CoO detected by XRD analysis and that therefore, cobalt would reduce with increasing temperature, which must be accompanied by an oxygen release.

The carbonation reaction mechanism of $NaCoO_2$ provided by Vera *et al.* is presented in the following:

$$3Co_2O_3 \rightarrow 2Co_3O_4 + 1/2O_2 \; 400\ ^\circ C < T < 700\ ^\circ C$$

$$Co_3O_4 \rightarrow 3CoO + 1/2O_2 \; T > 700\ ^\circ C$$

In this work, dynamical chemical reactions occurring during standard thermograms in CO_2 sorption analysis were analyzed. For this, synthesized $NaCoO_2$ was subjected to continuous heating at a ramp of 5 °C min^{-1} under a $CO_2:N_2$ gas flow. Fig. 5a displays the evolution of the X-ray diffraction patterns upon heating, and Fig. 5b shows the corresponding temperature evolution.

The contour plot of Fig. 5a sheds light on the high-temperature reactions taking place during CO_2 absorption, and reveals the occurrence of a single step process in which $NaCoO_2$ reacts to form Co_3O_4 and Na_2CO_3. Importantly, no Co_2O_3 is evidenced. Therefore, it can be stated that Co_2O_3 would not form as an intermediate compound previous to the formation of Co_3O_4, as it was claimed by previous authors. These findings are consistent with theoretical results,[44] which indicate that Co_2O_3 compound is thermodynamically highly unstable. Also, it must be remarked that the appearance of CoO phase is not observed from our experimental data, which corresponds to temperatures up to 750 °C. It is worth noting that the presented results do not contradict the previous reports by Vera *et al.*[20] since they have reported the presence of CoO only in samples that had been subjected to temperatures higher than 750 °C, which is the maximum temperature reached in this experiment.

Rietveld refinement results allowed to track the composition of the system in real time. The analysis of the XRD patterns during the CO_2 capture process was performed and is presented in Fig. 6. As it is possible to observe, $Na_{0.74}CoO_2$ remains stable until approximately 100 °C, temperature at which the absorption reaction starts. At this temperature, marked with a vertical dashed line in the figure, the formation of Co_3O_4 and Na_2CO_3 is observed. From Fig. 6 it is possible to see a previous jump in the reaction at t = 37 min. This is an artifact caused by the need to keep the temperature on hold for a long time due to a beam loss during the experiment (in Fig. 5 and 6 the time loss caused by the beam drop is compressed to make the figures more readable). The reaction keeps advancing very slowly until the system reaches 400 °C, temperature at which the reaction rate starts to grow. To make it easier to follow with the reaction, weight fractions were transformed into molar fractions using the following equation:

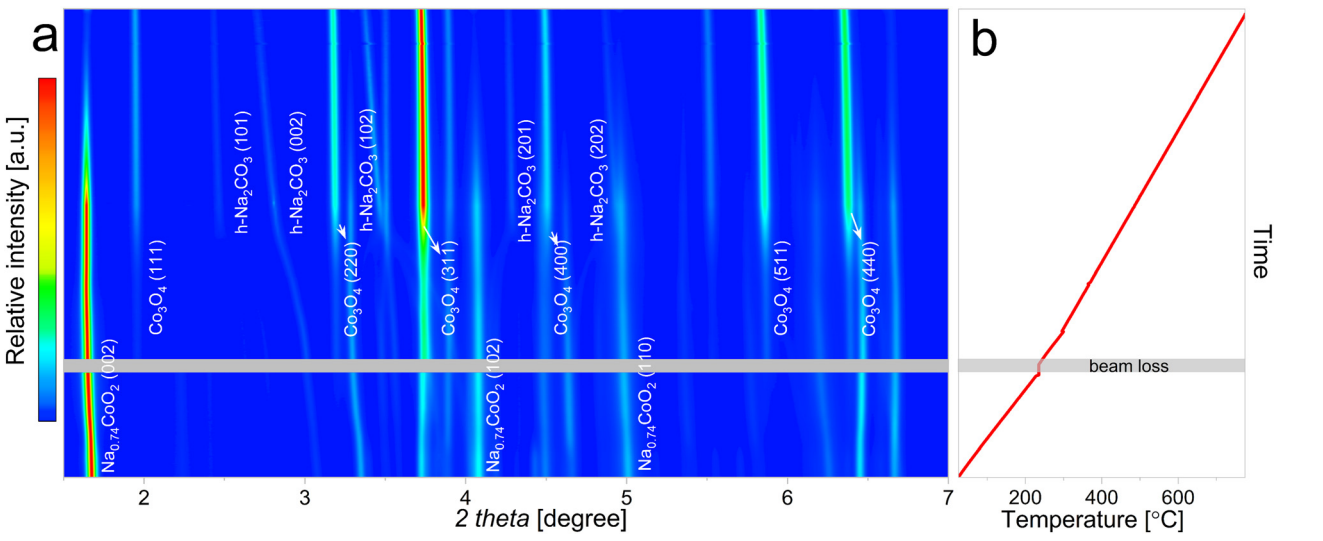

Fig. 5 a) Contour plot displaying XRD data corresponding to $NaCoO_2$ dynamic heating under CO_2 gas flow until 750 °C, b) temperature evolution during $NaCoO_2$ carbonation process.

$$x_a = \frac{w_a/M_a}{\sum_i w_i/M_i}$$

where x_a, w_a and M_a are the mole fraction, weight percent and molecular mass of the phase a respectively.

At 400 °C, the CO_2 capture rate increases until reaching 550 °C. At this temperature, the system CO_2 capture dynamics slows again showing an asymptotic behaviour. Previous works have reported that at temperatures under 400 °C there is process of surface adsorption, however our results indicate that at these temperatures there is already some formation of Co_3O_4 and Na_2CO_3. This is an indication that the actual process occurring is actually a chemisorption and that the reason why the reaction does continue is because of kinetic limitations.

Based on the time-resolved *in situ* results provided in this work, the proposed temperature-dependent reaction mechanism for $Na_{0.74}CoO_2$ carbonation process in the temperature range of 50 °C < T < 750 °C is the following:

$$4Na_{0.74}CoO_2 + 1.48CO_2 \rightarrow 1.48Na_2CO_3 + 1.33Co_3O_4 + 0.59O_2$$

The main difference between the proposed reaction mechanism and the one that has been proposed by previous authors is the absence of Co_2O_3 phase, which was not observed at any point during the absorption process.

3. Conclusions

In this work, we analyzed the solid-state synthesis of $NaCoO_2$ *via* two different routes. In the first route, the starting reactants were Na_2CO_3 and $CoCo_3{\cdot}nH_2O$, while in the second case powders of Co_3O_4 and Na_2CO_3 were used as precursors. In both cases, the starting powder mixtures were heated up from room temperature to 700–800 °C and the evolution of the chemical reactions taking place at high temperatures was tracked time-resolved synchrotron powder X-ray diffraction.

Results revealed that the synthesis of $NaCoO_2$ from Na_2CO_3 and $CoCo_3{\cdot}nH_2O$ involves a two step process, in which $CoCo_3{\cdot}nH_2O$ first decomposes to Co_3O_4 and CoO, and the latter readily reacts with oxygen, resulting in its rapid conversion to Co_3O_4. Then, Co_3O_4 reacts with Na_2CO_3 to form $NaCoO_2$. In the second route, $NaCoO_2$ is formed following a single step process from Na_2CO_3 and Co_3O_4. However, a reversible reaction of Co_3O_4 to form Co_2O_3 was evidenced. Co_2O_3 reaction product is unstable thermodynamically and therefore was rapidly converted to Co_3O_4. Overall, the second synthesis route allowed to obtain $NaCoO_2$ at the lowest temperature of 700 °C.

The CO_2 capture dynamics of the resulting $NaCoO_2$ was also analyzed in the temperature range from 30 °C to 750 °C by heating the sample under controlled CO_2 flow. Time-resolved *in situ* X-ray diffraction data allowed to propose a reaction mechanism for the gas–solid reaction in which $NaCoO_2$ reacts with CO_2 to form Na_2CO_3 and Co_3O_4 as solid reaction products. These results contradict the previously proposed reaction mechanism for $NaCoO_2$ carbonation reaction.

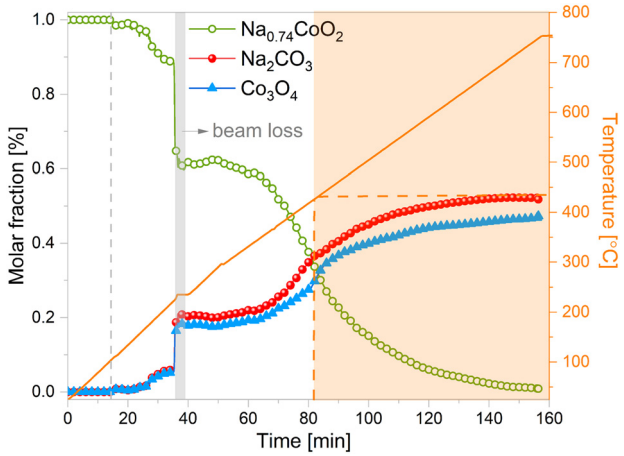

Fig. 6 Evolution of temperature and sample weight percent during $NaCoO_2$ carbonation reaction according to results from Rietveld analysis.

Conflicts of interest

There are no conflicts to declare.

Acknowledgements

The authors thank the European Synchrotron Radiation Facility for beamtime allocation, Florian Rusello and Tiago Couthinio are acknowledged for their help with the preparation of the experimental setup.

Notes and references

1 J. P. McCarty, *Conserv. Biol.*, 2001, **15**, 320–331.
2 K. L. O'Brien and R. M. Leichenko, *Glob. Environ. Change*, 2000, **10**, 221–232.
3 H. G. Bohle, T. E. Downing and M. J. Watts, *Glob. Environ. Change*, 1994, **4**, 37–48.
4 W. N. Adger and P. M. Kelly, *Mitig. Adapt. Strateg. Glob. Chang.*, 1999, **4**, 253–266.
5 Y. Zhang, Y. Gao, H. Pfeiffer, B. Louis, L. Sun, D. O'Hare and Q. Wang, *J. Mater. Chem. A*, 2019, **7**, 7962–8005.
6 S. Solomon, J. S. Daniel, T. J. Sanford, D. M. Murphy, G.-K. Plattner, R. Knutti and P. Friedlingstein, *Proc. Natl. Acad. Sci.*, 2010, **107**, 18354–18359.
7 A. Alonso, J. Moral-Vico, A. Abo Markeb, M. Busquets-Fité, D. Komilis, V. Puntes, A. Sánchez and X. Font, *Sci. Total Environ.*, 2017, **595**, 51–62.
8 M. T. Izquierdo, A. Saleh, E. Sánchez-Fernández, M. M. Maroto-Valer and S. García, *Ind. Eng. Chem. Res.*, 2018, **57**, 13802–13810.

9 K. Wang, W. Li, Z. Yin, Z. Zhou and P. Zhao, *Energy Fuels*, 2017, **31**, 6257–6265.
10 A. Nambo, J. He, T. Q. Nguyen, V. Atla, T. Druffel and M. Sunkara, *Nano Lett.*, 2017, **17**, 3327–3333.
11 Y. Hu, W. Liu, Y. Yang, M. Qu and H. Li, *Chem. Eng. J.*, 2019, **359**, 604–625.
12 P. Greim, A. A. Solomon and C. Breyer, *Nat. Commun.*, 2020, **11**, 4570.
13 V. L. Mejía-Trejo, E. Fregoso-Israel and H. Pfeiffer, *Chem. Mater.*, 2008, **20**, 7171–7176.
14 A. Sanna and M. M. Maroto-Valer, *Ind. Eng. Chem. Res.*, 2016, **55**, 4080–4088.
15 T. Cai, X. Chen, J. Zhong, Y. Wu, J. Ma, D. Liu and C. Liang, *Chem. Eng. J.*, 2020, **395**, 124139.
16 T. Zhao, E. Ochoa-Fernández, M. Rønning and D. Chen, *Chem. Mater.*, 2007, **19**, 3294–3301.
17 M. Z. Memon, G. Ji, J. Li and M. Zhao, *Ind. Eng. Chem. Res.*, 2017, **56**, 3223–3230.
18 E. Vera, B. Alcantar-Vazquez, Y. Duan and H. Pfeiffer, *RSC Adv.*, 2016, **6**, 2162–2170.
19 E. Vera, Y. Duan and H. Pfeiffer, *Energy Technol.*, 2019, **7**, 1980301.
20 E. Vera, B. Alcántar-Vázquez and H. Pfeiffer, *Chem. Eng. J.*, 2015, **271**, 106–113.
21 R. Molinder, T. P. Comyn, N. Hondow, J. E. Parker and V. Dupont, *Energy Environ. Sci.*, 2012, **5**, 8958–8969.
22 M. T. Dunstan, S. A. Maugeri, W. Liu, M. G. Tucker, O. O. Taiwo, B. Gonzalez, P. K. Allan, M. W. Gaultois, P. R. Shearing, D. A. Keen, A. E. Phillips, M. T. Dove, S. A. Scott, J. S. Dennis and C. P. Grey, *Faraday Discuss.*, 2016, **192**, 217–240.
23 A. Biasin, C. U. Segre and M. Strumendo, *Cryst. Growth Des.*, 2015, **15**, 5188–5201.
24 J. Manuel Valverde, A. Perejon, S. Medina and L. A. Perez-Maqueda, *Phys. Chem. Chem. Phys.*, 2015, **17**, 30162–30176.
25 J. M. Valverde and S. Medina, *Phys. Chem. Chem. Phys.*, 2017, **19**, 7587–7596.
26 M. V. Blanco, K. Kohopää, I. Snigireva and F. Cova, *Chem. Eng. J.*, 2018, **354**, 370–377.
27 F. Cova, G. Amica, K. Kohopää and M. V. Blanco, *Inorg. Chem.*, 2019, **58**, 1040–1047.
28 M. V. Blanco, P. M. Abdala, F. Gennari and F. Cova, *React. Chem. Eng.*, 2021, **6**, 1974–1982.
29 M. L. Grasso, M. V. Blanco, F. Cova, J. A. González, P. A. Larochette and F. C. Gennari, *Phys. Chem. Chem. Phys.*, 2018, **20**, 26570–26579.
30 B. V. R. Reddy, R. Ravikumar, C. Nithya and S. Gopukumar, *J. Mater. Chem. A*, 2015, **3**, 18059–18063.
31 P. Kehne, C. Guhl, Q. Ma, F. Tietz, L. Alff, R. Hausbrand and P. Komissinskiy, *J. Power Sources*, 2019, **409**, 86–93.
32 N. Bucher, S. Hartung, J. B. Franklin, A. M. Wise, L. Y. Lim, H.-Y. Chen, J. N. Weker, M. F. Toney and M. Srinivasan, *Chem. Mater.*, 2016, **28**, 2041–2051.
33 S. Hwang, Y. Lee, E. Jo, K. Y. Chung, W. Choi, S. M. Kim and W. Chang, *ACS Appl. Mater. Interfaces*, 2017, **9**, 18883–18888.
34 Y. Lei, X. Li, L. Liu and G. Ceder, *Chem. Mater.*, 2014, **26**, 5288–5296.
35 J. Kieffer and D. Karkoulis, *J. Phys.: Conf. Ser.*, 2013, **425**, 202012.
36 J. Rodriguez-Carvajal, *Phys. B*, 1993, **192**, 55–69.
37 C.-B. Wang, H.-K. Lin and C.-W. Tang, *Catal. Lett.*, 2004, **94**, 69–74.
38 H. Du, L. Jiao, Q. Wang, Q. Huan, L. Guo, Y. Si, Y. Wang and H. Yuan, *CrystEngComm*, 2013, **15**, 6101–6109.
39 A. Arakcheeva and G. Chapuis, *Acta Crystallogr., Sect. B: Struct. Sci.*, 2005, **61**, 601–607.
40 Y. J. Min, S.-M. Hong, S. H. Kim, K. B. Lee and S. G. Jeon, *Korean J. Chem. Eng.*, 2014, **31**, 1668–1673.
41 C. T. Lin, D. Chen, A. Maljuk and P. Lemmens, *J. Cryst. Growth*, 2006, **292**(2), 422–428.
42 N. S. Krasutskaya, A. I. Klyndyuk, L. E. Evseeva and S. A. Tanaeva, *Inorg. Mater.*, 2016, **52**, 393–399.
43 I. F. Gilmutdinov, I. R. Mukhamedshin, F. Rullier-Albenque and H. Alloul, *J. Phys. Chem. Solids*, 2018, **121**, 145–150.
44 P. N. Shanbhag, R. K. Biswas, S. K. Pati, A. Sundaresan and C. N. R. Rao, *ACS Omega*, 2020, **5**, 29009–29016.
45 F.-C. Kong, Y.-F. Li, C. Shang and Z.-P. Liu, *J. Phys. Chem. C*, 2019, **123**, 17539–17547.